Gate field effects on the topological insulator BiSbTeSe₂ interface

Cite as: Appl. Phys. Lett. **116**, 031601 (2020); https://doi.org/10.1063/1.5127065 Submitted: 08 September 2019 . Accepted: 07 January 2020 . Published Online: 22 January 2020







ARTICLES YOU MAY BE INTERESTED IN

Ferroelectric memory field-effect transistors using CVD monolayer MoS₂ as resistive switching channel

Applied Physics Letters 116, 033501 (2020); https://doi.org/10.1063/1.5129963

Acoustic holography using composite metasurfaces

Applied Physics Letters 116, 030501 (2020); https://doi.org/10.1063/1.5132629

Tunneling electroresistance effects in epitaxial complex oxides on silicon Applied Physics Letters 116, 032902 (2020); https://doi.org/10.1063/1.5133081





Gate field effects on the topological insulator BiSbTeSe₂ interface

Cite as: Appl. Phys. Lett. **116**, 031601 (2020); doi: 10.1063/1.5127065 Submitted: 8 September 2019 · Accepted: 7 January 2020 · Published Online: 22 January 2020







Shuanglong Liu,^{1,2} (D) Yang Xu,^{3,a)} Yun-Peng Wang,^{1,2,b)} (D) Yong P. Chen,^{3,4,5,6} James N. Fry,¹ (D) and Hai-Ping Cheng^{1,2,7,c)} (D)

AFFILIATIONS

- ¹Department of Physics, University of Florida, Gainesville, Florida 32611, USA
- ²Quantum Theory Project, University of Florida, Gainesville, Florida 32611, USA
- Department of Physics and Astronomy, Purdue University, West Lafayette, Indiana 47907, USA
- School of Electrical and Computer Engineering, Purdue University, West Lafayette, Indiana 47907, USA
- ⁵Birck Nanotechnology Center, Purdue University, West Lafayette, Indiana 47907, USA
- ⁶Purdue Quantum Science and Engineering Institute, Purdue University, West Lafayette, Indiana 47907, USA
- 7 Center for Molecular Magnetic Quantum Materials, University of Florida, Gainesville, Florida 32611, USA
- a) Present address: Applied and Engineering Physics, Cornell University, Ithaca, New York 14853, USA.
- b) Present address: School of Physical Science and Electronics, Central South University, Changsha, Hunan, 410012, China.
- c)Electronic mail: hping@ufl.edu

ABSTRACT

Interfaces between two topological insulators are of fundamental interest in condensed matter physics. Inspired by experimental efforts, we study interfacial processes between two slabs of BiSbTeSe₂ (BSTS) via first principles calculations. Topological surface states are absent for the BSTS interface in its equilibrium separation, but our calculations show that they appear if the inter-slab distance is greater than 6 Å. More importantly, we find that topological interface states can be preserved by inserting two or more layers of hexagonal boron nitride between the two BSTS slabs. In experiments, the electric current tunneling through the interface is insensitive to back gate voltage when the bias voltage is small. Using a first-principles based method that allows us to simulate the gate field, we show that at low bias, the extra charge induced by a gate voltage resides on the surface that is closest to the gate electrode, leaving the interface almost undoped. This provides clues to understand the origin of the observed insensitivity of transport properties to back voltage at low bias. Our study resolves a few questions raised in experiment, which does not yet offer a clear correlation between microscopic physics and transport data. We provide a road map for the design of vertical tunneling junctions involving the interface between two topological insulators.

Published under license by AIP Publishing. https://doi.org/10.1063/1.5127065

Topological surface states (TSSs) of a three dimensional topological insulator (TI) have drawn much research attention due to their robustness, linear dispersion, and spin-momentum locking, which allow potential applications in low-energy-consumption electronics and spin-tronics. ^{1,2} A large category of electronic/spintronic devices involves an interface between a TI and another material, which could be a normal insulator, metals, magnets, superconductors, or even molecules. ^{3–15} It is thus necessary to understand how TSSs are affected by proximity effects, especially their preservation ^{3–9} or passivation. ^{4,14,15} A gate field is often applied to control the electron transport properties of an electronic device. A single gate induces charge doping, and a dual gate configuration can further create a vertical electric field. A gate voltage provides a

knob for tuning topological surface/interface states. ^{16–18} Nevertheless, theoretical work has been mostly limited to model ^{19,20} or conventional electronic structure calculations. ^{21,22}

 ${\rm Bi}_x{\rm Sb}_{2-x}{\rm Te}_y{\rm Se}_{3-y}$ (BSTS) has been reported to be a topological insulator with high bulk resistivity and robust surface states for certain x and y values. ^{23–26} In this work, we study the interface between two BiSbTeSe₂ slabs, with and without spacers in between. We construct a theoretical approach that can simulate gate effects via a first-principles calculation. The major results reported here are from theoretical investigations, which are motivated by the experimental data. Experimentally, two BSTS flakes are prepared separately before being stacked together to form a vertical tunneling junction. It is observed that the electric current

is not sensitive to a back gate voltage when the bias voltage between the two BSTS slabs is small (see Fig. S1 in the supplementary material). Based on these observations, theoretical investigations focus on the three questions—first, do topological interface states exist at the BSTS interface? Second, how do topological interface states respond to a gate field when they are present? Third, how can we turn BSTS into a quantum system that is useful for future electronics? This work offers a picture at the electron level, deepens our understanding of TI interfaces, demonstrates a way to utilize quantum TSSs, and finally provides an idea for designing TI-based vertical tunneling devices.

In order to answer whether the interface hosts topological surface states, we first generate a special quasirandom structure of the BSTS alloy, which approximates the true disordered state with a periodic supercell, 27 using the "mcsqs" code of the Alloy Theoretic Automated Toolkit. 27,28 The topological invariants of our quasirandom BSTS supercell are calculated to be (1;0,0,0) with the aid of the Z2Pack package. 29,30 As such, our model BSTS represents a strong topological insulator. Then, we build a BSTS interface based on the special quasirandom structure and visualize it using the Visualization for Electronic and Structural Analysis (VESTA) software. 31 As shown in Fig. 1, the interface is made of two BSTS slabs that are separated by distance d,

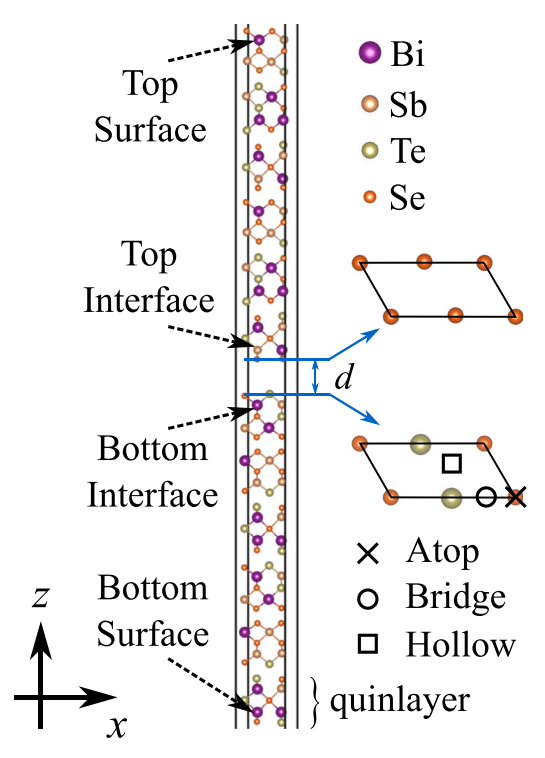


FIG. 1. Atomic configuration of the BSTS interface, consisting of two BSTS slabs. The two slabs are separated by a distance d, and each slab contains six quinlayers. The violet, ocher, olive, and orange balls represent Bi, Sb, Te, and Se, respectively. There are four "surfaces" in the system, denoted as the top surface, the bottom surface, the top interface, and the bottom interface, as indicated by the dashed black arrows. The interfacial atomic layers are zoomed in and shown by the side in a top view. Three stacking sites are marked in the interfacial atomic layer from the lower BSTS slab. The vertical solid lines are the boundaries of the unit cell. The interface is periodic in the x and y directions and perpendicular to the z direction.

where each slab contains six quinlayers, periodic in the x-y plane perpendicular to the z-direction. The in-plane lattice constants are a=8.390 Å and b=4.191 Å, with $\gamma=120^{\circ}$. At least 15 Å of vacuum is added along the z-direction to avoid interaction between periodic images of the same system. For a single BSTS slab with six quinlayers, we test that there are localized surface states with spin-momentum locking, which disappears if spin-orbit coupling is switched off, evidence that the special random structure represents a topological insulator. Our calculations are based on density functional theory as implemented in the Vienna Ab initio simulation package (VASP).^{34,35} In VASP calculations, we adopt an energy cutoff of at least 450 eV for plane waves, the PAW pseudopotential, 35,36 the optB86b vdW-DF energy functional for including the van der Waals interaction, $^{37-39}$ a 5 × 9 × 1 Monkhorst-Pack *k*-point mesh, an energy tolerance of 1×10^{-6} eV for self-consistency, and a force tolerance of 0.01 eV/Å for ionic relaxation.

Now, we examine the relation between interface states and the inter-slab distance d. Figures 2(a) and 2(b) show the band structure of the BSTS interface with inter-slab distances of 3.0 Å and 6.0 Å, respectively. For both d = 3.0 Å and d = 6.0 Å, the top (bottom) surface band forms a Dirac cone around the Fermi energy. In contrast, for $d = 3.0 \,\text{Å}$, the top (bottom) interface band does not form a Dirac cone, and an energy gap of $E_{\rm g} \approx 0.105\,{\rm eV}$ opens at the Γ point. This energy gap, however, closes when $d = 6.0 \,\text{Å}$, due to weak interaction between the two slabs, and accordingly, the Dirac cone for the top (bottom) interface is recovered. Therefore, the presence of topological interface states strongly depends on the inter-stab distance d. Figure 2(c) shows that E_g decreases with d and reaches zero at around 6 Å. Note that there are three typical alignments of stacking between the two BSTS slabs, namely, atop, bridge, and hollow. The above discussion is for the BSTS interface with atop stacking; however, it remains valid qualitatively for the other two stackings. The energetically favorable d for the atop (bridge and hollow) stacking is about 3.6 (2.9, 2.6) Å,

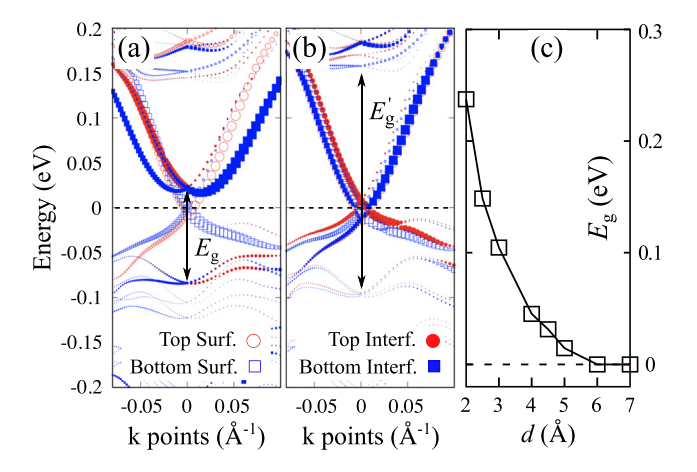


FIG. 2. Band structure for a BSTS interface with inter-slab distances of (a) $d=3.0\,\text{Å}$ and (b) $d=6.0\,\text{Å}$. The Fermi energy is set to zero. Each dot represents a Kohn–Sham state, with the size proportional to the projected density of states to the first quinlayer of a surface. Red empty (filled) circles are for the top surface (interface) states; blue empty (filled) squares are for the bottom surface (interface states. If a dot is bigger, the state is more localized on the corresponding surface/interface. $E_g\left(E_g'\right)$ is the energy gap for the interface (bulk) states at the Γ point. (c) E_g vs d for the BSTS interface.

and a Dirac cone is not formed. The hollow site stacking is the most stable configuration, about 0.08 eV and 0.30 eV lower than the bridge stacking and the atop stacking, respectively.

In order to recover TSSs at the interface, we considered inserting h-BN between the two BSTS slabs, since h-BN is a normal insulator and TSSs are known to exist at the interface between a topological insulator and a normal insulator³ (experimentally, it might be easier to prepare BSTS with a surface covered by an h-BN monolayer before stacking two pieces together). In the following, we show that monolayer h-BN is not sufficient, and two layers of h-BN are required. Figures 3(a) and 3(b) show the atomic configuration of the BSTS interface with monolayer (bilayer) h-BN, denoted as BSTS/1BN/BSTS (BSTS/2BN/BSTS). The band structures for BSTS/1BN/BSTS and BSTS/2BN/BSTS are shown in Figs. 3(c) and 3(d). The red circles (blue squares) are for the top (bottom) interface, and again, the size of a circle/square indicates the localization of the corresponding state. When there is only one layer of h-BN, a bandgap opens at the Γ point for both the top and the bottom interface states around the Fermi energy. In other words, the Dirac cone and TSS are absent at the interface. In contrast, when there are two layers of h-BN, the energy gap closes and two Dirac cones are formed around Fermi energy, one for the top interface states and the other for the bottom interface states. These results are for hollow stacking between BSTS and BN; however, they remain valid for atop stacking and bridge stacking. We observe

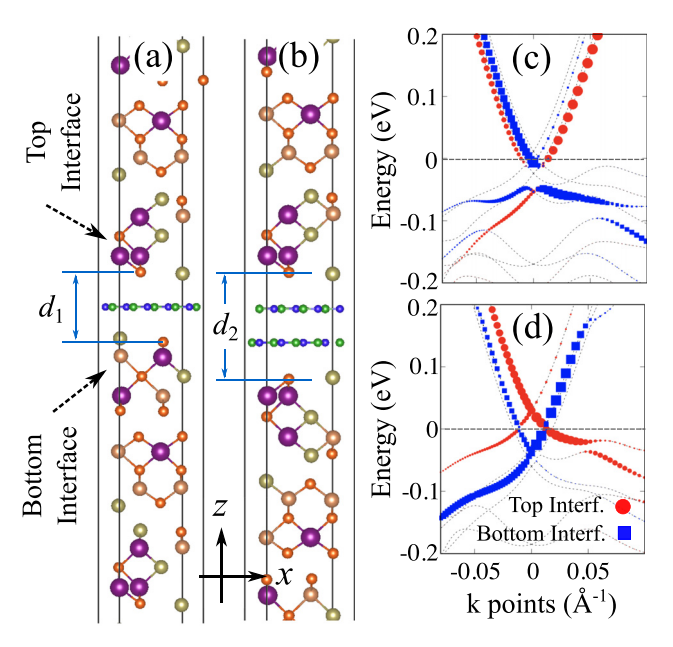


FIG. 3. Atomic configuration of the BSTS interface is shown with (a) monolayer h-BN and (b) bilayer h-BN. The optimized inter-slab distances are $d_1=7.04\,\text{Å}$ for panel (a) and $d_2=10.28\,\text{Å}$ for panel (b), as measured by the difference in the z-coordinate of the opposing Se atoms. Only the atoms close to the interface are shown although there are six quinlayers in each BSTS slab. The vertical lines are the boundaries of the unit cell. The band structure for the BSTS interface is shown for (c) monolayer h-BN and (d) bilayer h-BN. The red circles (blue squares) are for the top (bottom) interface states. If a red circle (blue square) is bigger, the corresponding state is more localized at the top (bottom) interface. The dashed lines show all energy bands within the energy range of $[-0.2:0.2]\,\text{eV}$. The Fermi energy is set to zero, as indicated by the horizontal gray line.

that the top (bottom) interface is slightly hole- (electron-) doped. This charge transfer arises from the asymmetry in the atomic configuration of the interface. If we construct an inversion symmetric interface, then the two Dirac cones indeed become identical and the Dirac points are located at the Fermi level. Note that the top and the bottom surface states still exist although they are not emphasized in Fig. 3.

So far, we have answered the question of whether or not TSSs exist at the BSTS interface. Now, we turn to the second question: How do topological interface states respond to a gate field? In order to answer this question, we take the BSTS/2BN/BSTS interface as an example and place it between two gate electrodes, as shown in Fig. 4. Each gate electrode has a constant Hartree potential, and the two gate electrodes could have different Hartree potentials, forming a nonperiodic boundary condition. We simulate the gate field effect using the Effective Screening Medium (ESM) method as implemented in the SIESTA package, 41,42 where the non-periodic boundary condition for the Hartree potential is dealt with Green's functions. A vacuum layer of about 1.2 nm thick is inserted between the BSTS slab and the top/ bottom gate electrode as a dielectric layer. We adopt norm-conserving relativistic pseudopotentials as generated via the Troullier-Martins scheme of the "ATOM" code. ^{43,44} The pseudopotentials for Bi, Se, and Te atoms are created by Rivero *et al.*, ⁴⁵ and the rest are created by the authors. The localized basis set is optimized in order to obtain a reasonable band structure compared to the results of VASP. We use the Perdew-Burke-Ernzerhof exchange correlation energy functional. This does not present a problem because the atomic structure is fixed

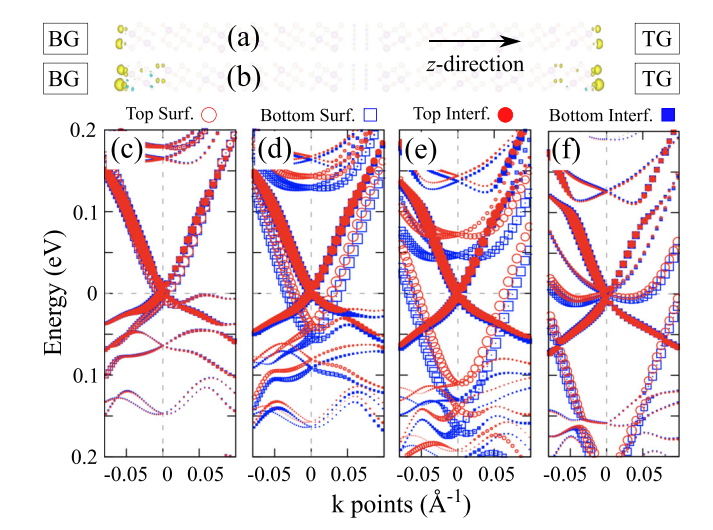


FIG. 4. Doping effects on the BSTS interface with bilayer h-BN. (a) Electron density difference $\rho(Q=-0.05,E=0)-\rho(Q=0,E=0)$, where $\rho(Q,E)$ is the electron density for the system with net charge Q (measured in unit charges) per cell under electric field E (V/Å). BG denotes the back gate electrode and TG the top gate electrode. (b) Electron density difference $\rho(Q=-0.10,E=0)-\rho(Q=0,E=0)$. The isosurface threshold for both (a) and (b) is 5×10^{-5} bohr $^{-3}$. Yellow (cyan) represents the positive (negative) charge density, gaining (losing) electrons. (c)–(f): Energy bands of the system with net charges of (c) Q=0, (d) Q=-0.0.0, and (f) Q=-0.10, per cell. The electric field E is zero for panels (c)–(f). The size of an empty/filled red circle is proportional to the local density of states of the local density of states of the bottom surface/interface.

and van der Waals interaction does not change the band structure much. A mesh cutoff of 150 Ry is used to sample in real space.

Two gate electrodes permit not only charge doping but also an electric field perpendicular to the interface. Here, the *electric field* means the average electric field between the two gate electrodes,

$$E = (V_H^{\text{TG}} - V_H^{\text{BG}})/L, \tag{1}$$

where $V_H^{\rm TG} - V_H^{\rm BG}$ is the Hartree potential difference between the top and bottom gate electrodes and L is the distance between the two gate electrodes. Electric field E in the caption of Fig. 4 also means that in Eq. (1). Figures 4(a) and 4(b) show the charge redistribution across the BSTS interface when it is doped with extra electrons 46 and subject to zero electric field. In Fig. 4(a), the BSTS interface with bilayer h-BN is doped with Q = -0.05 unit charges per unit cell. The corresponding carrier density $\sigma = Q/S$ is about -1.64×10^{13} cm⁻², where S is the surface area of a unit cell. As seen from the figure, the extra electrons are mainly located at the top and the bottom surfaces, while the inner part of the system is hardly doped. For a single gate configuration, the extra charge goes mainly to the surface that is closest to the gate electrode. As such, the local electronic structure at the interface does not change much, and it might be a reason for the insensitivity of the electric current to the gate voltage at small bias voltage. In Fig. 4(b), the net charge per cell is Q = -0.1. In this case, compared to Fig. 4(a), the extra electrons spread more into the inner part of the heterostructure. In order to understand this, we plot the band structures of the BSTS interface with different net charges in Figs. 4(c)-4(f). As shown in Fig. 4(c), without charge doping, there are four Dirac cones around the Fermi energy for the top surface, the top interface, the bottom interface, and the bottom surface. In Fig. 4(d), the system is doped with 0.03 electrons (Q = -0.03) per unit cell, and these electrons fill into the two Dirac cones for the top and the bottom surfaces, leaving the remaining two Dirac cones undoped. This is consistent with the charge redistribution shown in Fig. 4(a). It can also be seen from Fig. 4(d) that the bulk energy bands above the Fermi energy move downwards. At yet higher doping levels such as Q = -0.05 in Fig. 4(e), the surface energy bands are filled with more electrons and the bulk energy bands move even closer to the Fermi energy. Eventually, the bulk energy bands reach the Fermi energy and thus are also doped, as seen in Fig. 4(f) where Q = -0.10. At certain doping levels, the charge distribution of the BSTS interface with bilayer h-BN can be further tuned by the electric field E between the two electrodes. In the case of Q = -0.05, a small electric field along the z-direction moves electrons from the top surface to the bottom surface, and the inner part of the system is not doped until E is greater than 0.01 V/Å. This may be related to the increased sensitivity of the electric current to the gate voltage at higher bias voltages, as shown in Fig. S1 (see the supplementary material).

In conclusion, we have a clear microscopic picture of the interface between two slabs of the topological insulator $BiSbTeSe_2$. We find that topological interface states are absent unless the inter-slab distance is greater than 6 Å; they can, however, be preserved by two or more layers of h-BN that serve as a spacer between the two BSTS systems, which is verified by our calculations and is the answer to the third question imposed at the beginning of this paper. We undercover the mechanism underlying physical processes at small and large doping levels and provide clues to understand electron transport characteristics in the BSTS vertical tunneling junction configuration.

The combination of an *h*-BN spacer and single/double gating is a promising way to protect TSSs and modify interfacial electronic processes.

See the supplementary material for the electron transport measurement of a BSTS vertical tunneling junction, energy bands and hybrid Wannier charge centers of the quasirandom BSTS, the results for different stackings between a BSTS slab and another BSTS slab or a BN layer, the charge distribution for a single gate configuration, the effect of the electric field on the BSTS interface, parameters for the basis set and pseudopotentials, etc.

This work was supported by the U.S. Department of Energy (DOE), Office of Basic Energy Sciences (BES), under Contract No. DE-FG02-02ER45995. Y.P.C. acknowledges partial support from the National Science Foundation (NSF) under Grant No. EFMA-1641101. Computations were done using the utilities of the National Energy Research Scientific Computing Center and University of Florida Research Computing.

REFERENCES

Hsieh, Y. Xia, D. Qian, L. Wray, J. H. Dil, F. Meier, J. Osterwalder, L. Patthey, J. G. Checkelsky, N. P. Ong, A. V. Fedorov, H. Lin, A. Bansil, D. Grauer, Y. S. Hor, R. J. Cava, and M. Z. Hasan, Nature 460, 1101–1106 (2009).
Y. P. Chen, Proc. SPIE 8373, 83730B (2012).

³P. Gehring, B. F. Gao, M. Burghard, and K. Kern, Nano Lett. **12**, 5137–5142 (2012).

⁴M. H. Berntsen, O. Götberg, B. M. Wojek, and O. Tjernberg, Phys. Rev. B 88, 195132 (2013).

⁵R. Yoshimi, A. Tsukazaki, K. Kikutake, J. G. Checkelsky, K. S. Takahashi, M. Kawasaki, and Y. Tokura, Nat. Mater. 13, 253–257 (2014).

⁶C. Seibel, H. Maaß, M. Ohtaka, S. Fiedler, C. Jünger, C.-H. Min, H. Bentmann, K. Sakamoto, and F. Reinert, Phys. Rev. B 86, 161105(R) (2012).

⁷N. Kim, P. Lee, Y. Kim, J. S. Kim, Y. Kim, D. Y. Noh, S. U. Yu, J. Chung, and K. S. Kim, ACS Nano 8, 1154–1160 (2014).

⁸M. R. Scholz, J. Sánchez-Barriga, D. Marchenko, A. Varykhalov, A. Volykhov, L. V. Yashina, and O. Rader, Phys. Rev. Lett. 108, 256810 (2012).

⁹T. Shoman, A. Takayama, T. Sato, S. Souma, T. Takahashi, T. Oguchi, K. Segawa, and Y. Ando, Nat. Commun. 6, 6547 (2015).

¹⁰ J. Li, Z. Y. Wang, A. Tan, P.-A. Glans, E. Arenholz, C. Hwang, J. Shi, and Z. Q. Qiu, Phys. Rev. B 86, 054430 (2012).

¹¹M. Li, C.-Z. Chang, B. J. Kirby, M. E. Jamer, W. Cui, L. Wu, P. Wei, Y. Zhu, D. Heiman, J. Li, and J. S. Moodera, Phys. Rev. Lett. 115, 087201 (2015).

¹²L. Fu and C. L. Kane, Phys. Rev. Lett. **100**, 096407 (2008).

¹³L. A. Jauregui, M. Kayyalha, A. Kazakov, I. Miotkowski, L. P. Rokhinson, and Y. P. Chen, Appl. Phys. Lett. 112, 093105 (2018).

¹⁴J. Zhang, J. P. Velev, X. Dang, and E. Y. Tsymbal, Phys. Rev. B **94**, 014435 (2016).

¹⁵S. Jakobs, A. Narayan, B. Stadtmúller, A. Droghetti, I. Rungger, Y. S. Hor, S. Klyatskaya, D. Jungkenn, J. Stöckl, M. Laux, O. L. A. Monti, M. Aeschlimann, R. J. Cava, M. Ruben, S. Mathias, S. Sanvito, and M. Cinchetti, Nano Lett. 15, 6022–6029 (2015).

¹⁶H. Steinberg, D. R. Gardner, Y. S. Lee, and P. Jarillo-Herre, Nano Lett. 10, 5032–5036 (2010).

¹⁷A. Sulaev, M. Zeng, S.-Q. Shen, S. K. Cho, W. G. Zhu, Y. P. Feng, S. V. Eremeev, Y. Kawazoe, L. Shen, and L. Wang, Nano Lett. 15, 2061–2066 (2015).

¹⁸Y. Xu, I. Miotkowski, and Y. P. Chen, Nat. Commun. 7, 11434 (2016).

¹⁹J. Li and K. Chang, Appl. Phys. Lett. **95**, 222110 (2009).

20T. Yokoyama, A. V. Balatsky, and N. Nagaosa, Phys. Rev. Lett. 104, 246806 (2010).

²¹H. Min, B. Sahu, S. K. Banerjee, and A. H. MacDonald, Phys. Rev. B 75, 155115 (2007)

- ²²M. Houssa, B. van den Broek, K. Iordanidou, A. K. Augustin Lu, G. Pourtois, J.-P. Locquet, V. Afanas'ev, and A. Stesmans, Nano Res. 9, 774–778 (2016).
- ²³A. A. Taskin, Z. Ren, S. Sasaki, K. Segawa, and Y. Ando, Phys. Rev. Lett. 107, 016801 (2011).
- ²⁴T. Arakane, T. Sato, S. Souma, K. Kosaka, K. Nakayama, M. Komatsu, T. Takahashi, Z. Ren, K. Segawa, and Y. Ando, Nat. Commun. 3, 636 (2012).
- 25Y. Xu, I. Miotkowski, C. Liu, J. Tian, H. Nam, N. Alidoust, J. Hu, C.-K. Shih, M. Z. Hasan, and Y. P. Chen, Nat. Phys. 10, 956–963 (2014).
- ²⁶H. Lohani, P. Mishra, A. Banerjee, K. Majhi, R. Ganesan, U. Manju, D. Topwal, P. S. Anil Kumar, and B. R. Sekhar, Sci. Rep. 7, 4567 (2017).
- ²⁷A. van de Walle, P. Tiwary, M. de Jong, D. L. Olmsted, M. Asta, A. Dick, D. Shin, Y. Wang, L.-Q. Chen, and Z.-K. Liu, CALPHAD J. 42, 13–18 (2013).
- ²⁸A. van de Walle, M. Asta, and G. Ceder, CALPHAD J. 26, 539–553 (2002).
- ²⁹D. Gresch, G. Autès, O. V. Yazyev, M. Troyer, D. Vanderbilt, B. A. Bernevig, and A. A. Soluyanov, Phys. Rev. B 95, 075146 (2017).
- 30 A. A. Soluyanov and D. Vanderbilt, Phys. Rev. B 83, 235401 (2011).
- ³¹K. Momma and F. Izumi, J. Appl. Crystallogr. **44**, 1272–1276 (2011).
- 32P. Hohenberg and K. Walter, Phys. Rev. 136, B864–B871 (1964).
- ³³W. Kohn and L. J. Sham, Phys. Rev. **140**, A1133–A1138 (1965).
- ³⁴G. Kresse and J. Hafner, Phys. Rev. B **47**, 558 (1993).

- ³⁵G. Kresse and D. Joubert, Phys. Rev. B **59**, 1758 (1999).
- ³⁶P. E. Blöchl, Phys. Rev. B **50**, 17953 (1994).
- ³⁷M. Dion, H. Rydberg, E. Schröder, D. C. Langreth, and B. I. Lundqvist, Phys. Rev. Lett. **92**, 246401 (2004).
- ³⁸G. Román-Pérez and J. M. Soler, Phys. Rev. Lett. **103**, 096102 (2009).
- ⁵⁹J. Klimeš, D. R. Bowler, and A. Michaelides, J. Phys.: Condens. Matter 22, 022201 (2010).
- ⁴⁰W. Auwärter, H. U. Suter, H. Sachdev, and T. Greber, Chem. Mater. 16, 343–345 (2004).
- ⁴¹M. Otani and O. Sugino, Phys. Rev. B 73, 115407 (2006).
- ⁴²J. M. Solar, E. Artacho, J. D. Gale, A. García, J. Junquera, P. Ordeón, and D. Sánchez-Portal, J. Phys.: Condens. Matter 14, 2745 (2002).
- 43N. Troullier and J. L. Martins, Phys. Rev. B 43, 1993 (1991).
- 44ATOM, a program for DFT calculations in atoms and pseudopotential generation maintained by Alberto Garcia.
- 45P. Rivero, V. M. García-Suárez, D. Pereñiguez, K. Utt, Y. Yang, L. Bellaiche, K. Park, J. Ferrer, and S. Barraza-Lopez, Comput. Mater. Sci. 98, 372–389 (2015)
- 46Since the TSSs below the Fermi energy are not very accurate in SIESTA compared to VASP, we will consider only electron doping in the following.